MATRIX-FREE CONTINUATION OF LIMIT CYCLES AND THEIR BIFURCATIONS FOR A DUCTED PREMIXED FLAME

Iain C. Waugh*[1] †, Karthik Kashinath[1], Matthew P. Juniper[1]

[1] Cambridge University Engineering Department, Trumpington Street,Cambridge, CB2 1PZ, United Kingdom
* Corresponding author: icw26@cam.ac.uk

To define the nonlinear behaviour of a thermoacoustic system, it is important to find the regions of parameter space where limit cycles exist, and furthermore, to find the regions where the period-1 limit cycles bifurcate to period-2^n, quasiperiodic or chaotic behaviour. In an earlier study we have shown that matrix-free continuation methods can efficiently calculate the limit cycles of large thermoacoustic systems. This paper demonstrates that these continuation methods can also calculate the bifurcations to the limit cycles and show which coupled flame-acoustic motion causes the qualitative change in behaviour.

The matrix-free methods are demonstrated on a model of a ducted axisymmetric premixed flame, using a kinematic G-equation solver. The methods find limit cycles and period-2 limit cycles, and fold, period-doubling and Neimark-Sacker bifurcations as a function of the location of the flame in the duct, and the aspect ratio of the steady flame.

Premixed flames have been shown to exhibit periodic, period-2, quasiperiodic and chaotic behaviour in both experiments [1, 2, 3, 4] and numerical simulations [5, 6, 7]. The existence of these nonlinear behaviours is often a strong function of the system's parameters and the acoustic amplitude. As parameters vary there may be a sharp change in system behaviour. This could be because the dominant nonlinear behaviour ceases to exist (such as after a fold bifurcation), or this could be because there is a region of multistability, and the system has switched mode [7]. In the thermoacoustic literature there is little explanation, however, of why the qualitative behaviour of the system changes at a given parameter-amplitude combination.

Limit cycles can be found numerically using frequency domain or time domain techniques. Thermoacoustic limit cycles are commonly estimated using frequency domain techniques, such as the Flame Describing Function (FDF) [8]. Frequency domain techniques can estimate the location of fold bifurcations, where a limit cycle becomes unstable [9]. They cannot estimate the location of period-doubling or Neimark-Sacker bifurcations, however, because these bifurcations occur when a second frequency becomes unstable.

Frequency domain techniques can only consider one frequency at once. Time domain techniques do not have this limitation and can calculate both limit cycles and their bifurcations. In the time domain, brute force timemarching has been used to find parameter regions where a ducted premixed flame model exhibits period-1, period-2^n, frequency locked, quasiperiodic and chaotic behaviour [7], and to examine these attractors in phase space. In particular, this study highlighted the importance of unstable attractors in mode switching. Brute force timemarching has several limitations. First, it is computationally expensive because it may take a long time for the system to settle to an attractor. Second, the system will converge only to stable attractors (although it may remain long enough near an unstable attractor for its amplitude to be estimated using the time series). Third, the time series alone cannot explain why there is a qualitative behavioural change between parameter regions.

† Supported by EPSRC and IMechE funding

Continuation analysis is a time domain technique that tracks solutions as a function of system parameters. These solutions can be fixed points, limit cycles or bifurcations. For limit cycles, continuation analysis can improve on brute force timemarching: it converges to limit cycles much faster, it can converge to both stable and unstable cycles, and it can find the bifurcations to the limit cycles and therefore explain why the behaviour changes. Bifurcations occur when one coupled motion ('mode') changes in stability, which is defined by the eigenvalues of a suitable linearisation. The eigenvector then defines the coupled flame-acoustic motion ('mode') that causes the change in system behaviour. If this motion is known, then suitable control or damping could be designed such that the bifurcation either does not occur, or occurs in a more convenient parameter region. In an earlier paper, we have shown that matrix-free continuation methods are efficient for finding limit cycles of large thermoacoustic systems [10]. These methods were demonstrated on a model of a ducted diffusion flame. The model was found to be only weakly nonlinear, however, and therefore it did not display period-2^n or quasiperiodic behaviour. In this paper, the methods are demonstrated on a model of a ducted axisymmetric premixed flame, using a kinematic G-equation solver. The methods find period-1 and period-2 limit cycles, and fold, period-doubling and Neimark-Sacker bifurcations as a function of two system parameters: the location of the flame in the duct, and the aspect ratio of the steady flame. The matrix-free methods and their numerics are covered in depth in Ref. [10], and will therefore not be repeated here. Further details about the numerical implementation of the premixed flame model, and the incorporation of the matrix-free methods are included in Ref. [11].

1 Model description

The ducted premixed flame model consists of an axisymmetric flame domain coupled to a 1D acoustic duct. The flame domain uses the kinematic G-equation and a level set method to advect the flame shape. The model of the acoustic duct is the same as that used in Refs. [12, 13], and is discretised using Galerkin modes. Using the non-dimensionalisations $u = \frac{\tilde{u}}{\tilde{u}_0}, p = \frac{\tilde{p}}{\gamma M \tilde{p}_0}$, $x = \frac{\tilde{x}}{\tilde{L}_0}, t = \frac{\tilde{t}\tilde{c}_0}{\tilde{L}_0}$, the non-dimensional momentum and energy equations for the acoustic velocity and pressure are:

$$\begin{aligned} \frac{\partial u}{\partial t} + \frac{\partial p}{\partial x} &= 0 \\ \frac{\partial p}{\partial t} + \frac{\partial u}{\partial \tilde{x}} + \zeta p - \beta_T \dot{Q} \delta\left(x - x_f\right) &= 0 \end{aligned}$$

where:

$$\beta_T = \frac{\left(\gamma - 1\right)\tilde{\dot{Q}}_0 \alpha}{\gamma \tilde{p}_0 \tilde{u}_0} \quad \text{and} \quad \dot{Q} = \frac{\tilde{\dot{Q}}}{\tilde{\dot{Q}}_0}$$

Premixed flames propagate in a direction that is normal to the local flame surface. This paper uses the G-equation method in the flame domain, where the flame surface is defined as the zero contour of a scalar field and the flame normals are defined by the local gradient of the scalar field. Using a rotating boundary condition at the base of the flame, the G-equation model in this paper can simulate flame flashback, flame base motion, pinch-off and the formation of cusps. The evolution of the G-field in time is given by:

$$\frac{\partial G}{\partial t} + \underline{U} \cdot \underline{\nabla G} - s_L \left|\underline{\nabla G}\right| = 0 \tag{1}$$

where s_L is the flame speed, and $\underline{U}$ is the velocity vector in the flame field. The flame speed in this paper is dependent on curvature, because otherwise the G-equation forms unphysically sharp cusps. For a conical flame of aspect ratio β, the flame speed is given by:

$$s_L = \frac{u_0}{\sqrt{1+\beta^2}}\left(1 + M_\kappa \kappa_{axi}\right)$$

where M_κ is a non-dimensionalised Markstein length and κ_{axi} is the signed axisymmetric curvature. Strain effects are not included in the flame speed because it is not appropriate with the current velocity model. Because curvature is a second order quantity, however, adding curvature effects requires a significant drop in timestep to ensure that the CFL condition is met, and therefore timemarching is significantly slower.

When the equivalence ratio is fixed across the domain, and the domain is axisymmetric, the heat release rate is given by:

$$\dot{Q}_{axi} = \rho s_{L0}(\phi) h_R(\phi) \int_D 2\pi r (1 + M_\kappa \kappa_{axi}) \left|\underline{\nabla G}\right| \delta(G) \, dr \, dz \tag{2}$$

The G-equation is simulated using a modified version of the LSGEN2D code developed by Hemchandra (IISc Bangalore)[14], who used it to analyse the response of premixed flames to acoustic forcing [15] and to equivalence ratio fluctuations [16]. The code uses a local level-set method, a fifth order Weighted Essentially Non Oscillatory (WENO) procedure to take derivatives [17], and in this study, the HCR-2 method of Hartmann is used to reinitialise the G-field [18].

A simple velocity model is applied to the flame domain. Experiments on premixed flames have shown that acoustic perturbations cause travelling waves to advect down the flame [19]. The travelling waves typically advect more slowly than the mean flow. In this paper, the 1D advection equation propagates the acoustic disturbance at the burner downstream [15, 5, 20]. The velocity field is therefore simply the time history of the acoustic perturbation at the burner lip; the further from the burner lip, the further back in time that the acoustic disturbance was generated. The transverse velocity is determined by satisfying continuity. The acoustic disturbance travels a speed of u_0/K, where K is a parameter set typically between 1.0 and 1.5 [21]. The value of K has been demonstrated in numerical studies to have a strong effect on the nonlinear behaviour of premixed flames [5]. In particular, subcritical Hopf bifurcations are more prevalent at high values of K, and there are more parameter regions that have multiple limit cycles at different amplitudes and frequencies.

The velocity model produces flame shapes that look similar to those seen in experiments using a relatively simple formulation. This velocity model gives rise to some non-physical behaviour, however, such as that the mean heat release rate decreases as the forcing amplitude increases.

In this paper, there are several simplifications in thermoacoustic model: there is no temperature jump in the duct, the flame is considered compact, the acoustic damping model is based on simple coefficients at particular frequencies, the velocity model changes the mean heat release rate and does not allow for flame stretch, and the $(1 + M\kappa)$ term was not included in the heat release integral (equation 2). With these simplifications, the model shows the same qualitative behaviour as comparable experiments [1], but would not be suitable for quantitative comparisons.

The aim of this paper is to demonstrate that the continuation algorithms can efficiently map the nonlinear dynamics of a thermoacoustic system with a premixed flame model, by finding limit cycles and bifurcations to the limit cycles. The results in the next section demonstrate this well using the simplified thermoacoustic model.

2 Results

The matrix-free continuation methods were used to generate a bifurcation surface of limit cycles as two parameters are varied: the flame location in the duct, x_f, and the aspect ratio of the flame, $\beta = \sqrt{\left(\frac{u_0}{s_L}\right)^2 - 1}$. The parameters that are held fixed are: $\phi = 1.0$, $\alpha = 0.7$, $K = 1.5$, $M_\kappa = 0.04$, $L_0 = 1$, $\rho_0 = 1.16 kg/m^3$, $p_0 = 10^5$Pa, $\gamma = 1.4$, and acoustic damping factors $c_1 = 0.012$ and $c_2 = 0.024$[1] . The G-field is discretised on a 401×401 grid with spacing 0.005 and local level set regions 12 grid cells wide. A timestep

[1] It should be noted that there is a slight inconsistency with these damping values - which are dependent on the duct dimensions, R_0, L_0 - and the flame parameters, which set a physical flame size through the flame speed, and the ratio R_f/R_0 through α. For a consistent set of parameters, c_1 should be set slightly lower, and c_2 set slightly higher. Because the damping model in the acoustics is already basic, and the results of this paper are not used for quantitative comparisons this discrepancy was considered acceptable.

of 1.5×10^{-4} is used with 14 reinitialisation steps per timestep, with reinitialisation Courant number of 0.5. Twenty Galerkin modes are used for the acoustics.

2.1 Bifurcation surfaces

Figure 1 shows the bifurcation surface of period-1 limit cycles, whose frequency is close to that of the fundamental acoustic mode. The surface has regions with unstable limit cycles (dashed gray lines) and regions with stable limit cycles (solid black lines), whose boundaries are defined by the location of the period-doubling bifurcation (red line) and the Neimark-Sacker bifurcation (magenta line). The surface is shown only for realistic flame aspect ratios in the region $2 < \beta < 6$, and when the flame is in the first half of the acoustic duct, $x_f < 0.5$.

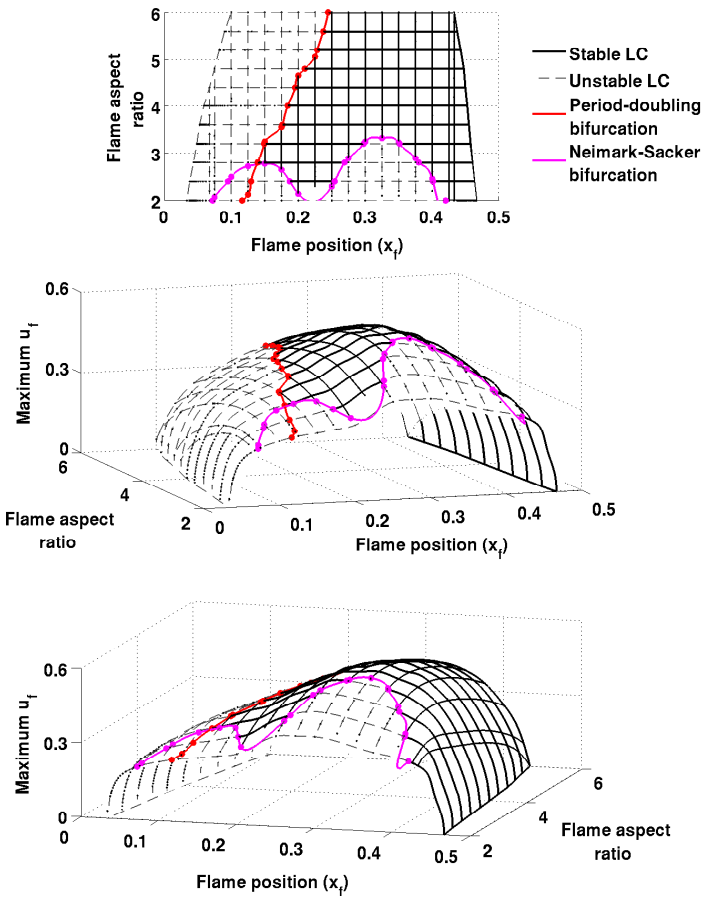

Figure 1: Bifurcation surface of period-1 limit cycles, as two parameters are varied: the flame location in the duct, x_f, and the flame aspect ratio, β. The surface is composed of over 600 limit cycles each converged to $||\underline{x}(0) - \underline{x}(T)|| < 5 \times 10^{-4}$. The z-axis is the maximum acoustic velocity at the flame. The surface has regions with unstable limit cycles (dashed gray lines) and regions with stable limit cycles (solid black lines), whose boundaries are defined by the location of the period-doubling bifurcation (red line) and the Neimark-Sacker bifurcation (magenta line). Subfigure (a) shows the surface from above, and subfigures (b) and (c) show the same 3D surface from two different views.

Figure 2 shows the bifurcation surface of period-2 limit cycles, whose frequency is close to half that of the fundamental acoustic mode. The surface shows the maximum velocity value at the flame during the limit cycle - this is one of several surfaces that show the period-2 cycle (see Figure 3). The surface

has regions with unstable limit cycles (dashed blue lines and gray shading) and regions with stable limit cycles (solid blue lines), whose boundaries are defined by the location of the period-doubling bifurcation (red line) and the fold bifurcation (green line). The period-doubling bifurcation is the same as that on the period-1 surface (Figure 1). The surface is shown for the same parameter range as Figure 1. The fold bifurcation exists at high β but its location is unresolved.

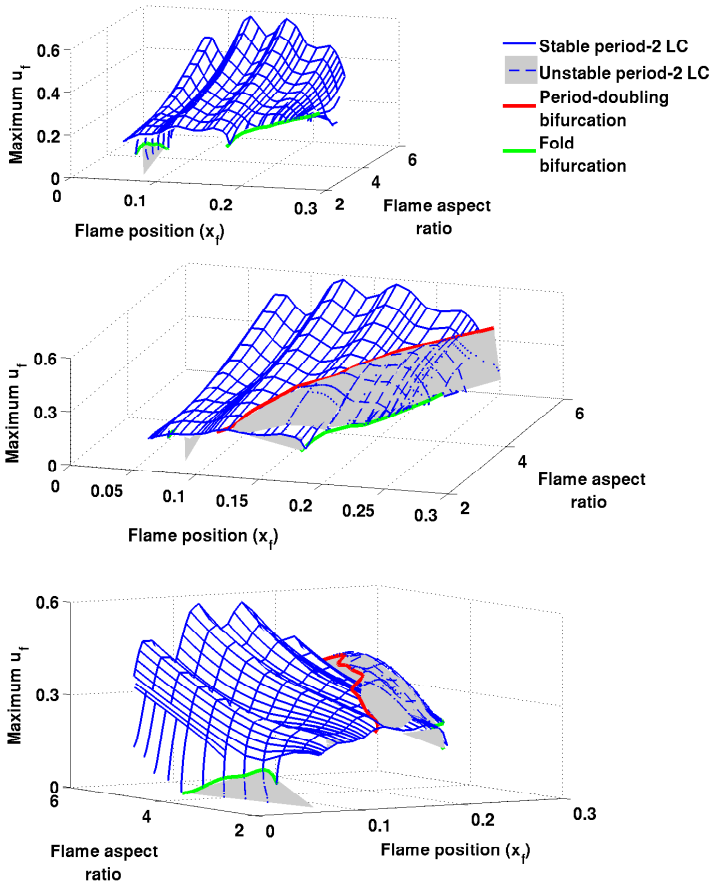

Figure 2: Bifurcation surface of period-2 limit cycles, as two parameters are varied: the flame location in the duct, x_f, and the flame aspect ratio, β. The surface is composed of over 1200 limit cycles each converged to $||\underline{x}(0) - \underline{x}(T)|| < 5 \times 10^{-4}$. The surface has regions with unstable limit cycles (dashed blue lines and gray shading) and regions with stable limit cycles (solid blue lines), whose boundaries are defined by the location of the fold bifurcation (green line) and the location of the period-doubling bifurcation (red line) - which is the same as that in Figure 1. Subfigure (a) shows does not show the unstable limit cycle surface; subfigures (b) and (c) show both the stable and unstable limit cycle surfaces from two different views.

Figures 1 and 2 only show the amplitude of the velocity fluctuation during the limit cycles. For the period-2 cycles, more information can be gained by plotting both the peaks and the troughs of the time series during the limit cycle. This is how the experimental results of Kabiraj [1] and the computational results of Kashinath [7] are presented. Figure 3 shows a 2D slice of the combined period-1 and period-2 bifurcation surfaces, taken at $\beta = 4$, with the y-axis showing both the peaks and the troughs of the limit cycles.

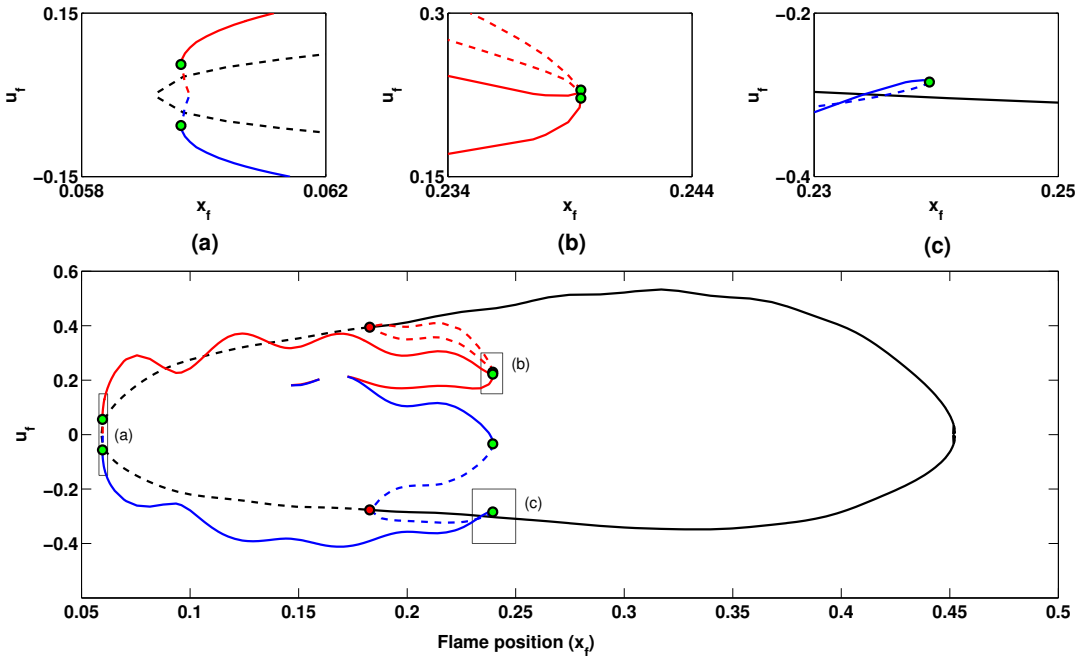

Figure 3: 2D slice of the combined period-1 and period-2 bifurcation surfaces, taken at $\beta = 4$. The y-axis plots the peaks and troughs of the velocity time series: period-1 peaks and troughs are shown in black, period-2 peaks are shown in red and period-2 troughs in blue. A solid line represents a stable limit cycle; a dashed line represents an unstable limit cycle. The period-doubling bifurcation is shown as a red dot; the fold bifurcations are shown as green dots.

The period-1 cycles (black) have only one peak and one trough, and these are not symmetric about zero - the velocity peak has a larger magnitude than the velocity trough. The period-2 peaks (red) and period-2 troughs (blue) form a more complicated shape. At some locations the period-2 cycles have two peaks and two troughs ($0.15 < x_f < 0.16, 0.17 < x_f$), and at other locations the period two cycles have only one peak and one trough ($x_f < 0.15, 0.16 < x_f < 0.17$). This difference occurs because the period-2 cycles are composed of two frequencies, whose relative magnitudes change along the period-2 branch (see next section). As the period-2 branch approaches the period-doubling bifurcation, the two peaks and two troughs close together. The period-doubling bifurcation is subcritical: the period-2 cycles emerging from it are unstable, and overlap with the stable period-1 limit cycle. There is therefore a region of bistability between $0.182 < x_f < 0.240$, where four attractors exist: a stable period-1 limit cycle, a stable period-2 limit cycle, an unstable period-2 limit cycle, and an unstable fixed point.

It is important to note that there are only two fold bifurcations on Figure 3 - the four green dots at $x_f = 0.240$ are not four separate fold bifurcations, they are a single fold bifurcation acting simultaneously on the four separate traces. The same is true of the two green dots at $x_f = 0.06$.

The period-2 peaks and troughs on Figure 3 oscillate with a wavelength of $\Delta x_f = 0.1$, which matches the wavelength of the twentieth Galerkin mode (only twenty were considered). This is probably an indication that a larger number of Galerkin modes are required in the discretisation. Including more Galerkin modes would probably smooth the peaks and troughs, but would probably not qualitatively change the behaviour [7].

2.2 Limit cycles

Once the limit cycles have been found by the continuation methods, their form can then be analysed. At an operating condition of $x_f = 0.195$ and flame aspect ratio 4 (Figure 3), there are three limit cycles: a stable period-1 limit cycle, an unstable period-2 limit cycle and a stable period-2 limit cycle. All three of these cycles have comparable velocity amplitudes at the flame. In this section, the form and spectra

of these three limit cycles are compared.

Figure 4a shows snapshots of the flame during the stable period-1 limit cycle. The flame shapes are qualitatively similar to those seen in experimental axisymmetric flames [19]. In particular, it was found that including curvature effects was important if flame shapes are to be compared with experimental ones. Without curvature the cusps become too sharp, especially at the centreline.

Figure 4b shows the time traces and spectra of the acoustic velocity and pressure at the flame, and the heat release of the flame. The heat release time trace is not sinusoidal; it contains a significant amount of higher harmonics. This will always be true when there are cusps on the flame surface.

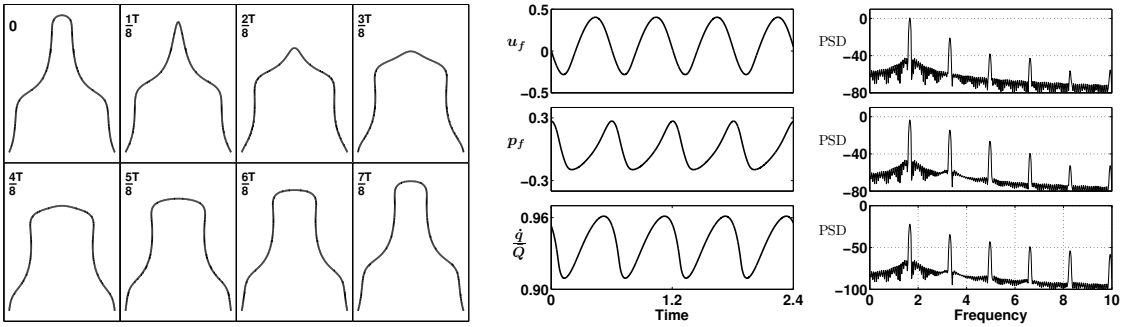

(a) (b)

Figure 4: Snapshots of the flame surface (a) and time traces and spectra (b) for the stable period-1 limit cycle at $x_f = 0.195$, with steady state flame aspect ratio of 4.

Near the period-doubling bifurcation, the period-2 cycles have a particular form where the cusps alternate position during the first and second halves of the cycle. Figure 5 shows the equivalent of Figure 4, but for the unstable period-2 limit cycle. The black lines show the flame shape during the first half of the cycle and the gray lines show the flame shape during the second half of the cycle. Because this is a period-2 limit cycle, a peak has appeared on the spectra at 0.9, which is half the frequency of the fundamental acoustic mode.

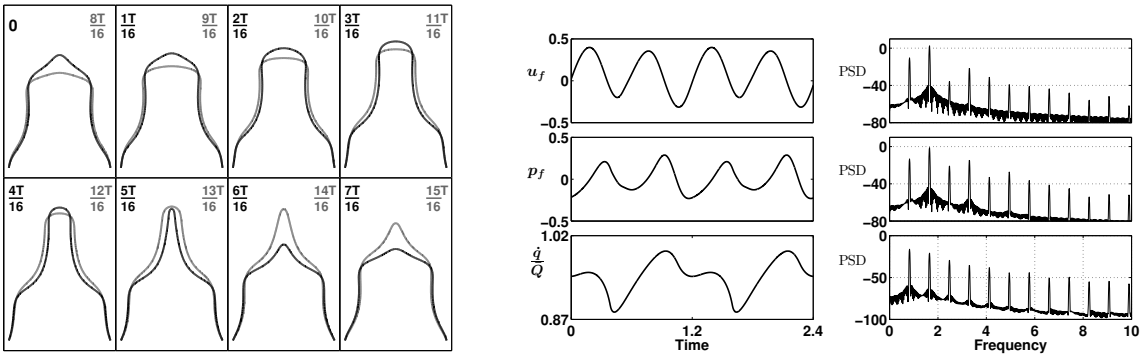

(a) (b)

Figure 5: Snapshots of the flame surface (a) and time traces and spectra (b) for the unstable period-2 cycle at $x_f = 0.195$, with steady state flame aspect ratio of 4. The time scale is the same as Fig. 4.

When further from the period-doubling bifurcation, however, it is more difficult to identify that the cycle is part of the period-2 branch, and not just a limit cycle with half the frequency of the fundamental acoustic mode - the peaks of the time trace lose the characteristic one-up, one-down structure that is commonly associated with period-2 cycles. In other words, the half-frequency starts to dominate, and

the flame shape does not alternate between the two halves of the cycle. Figure 6b shows an example of this, for the stable period-2 cycle.

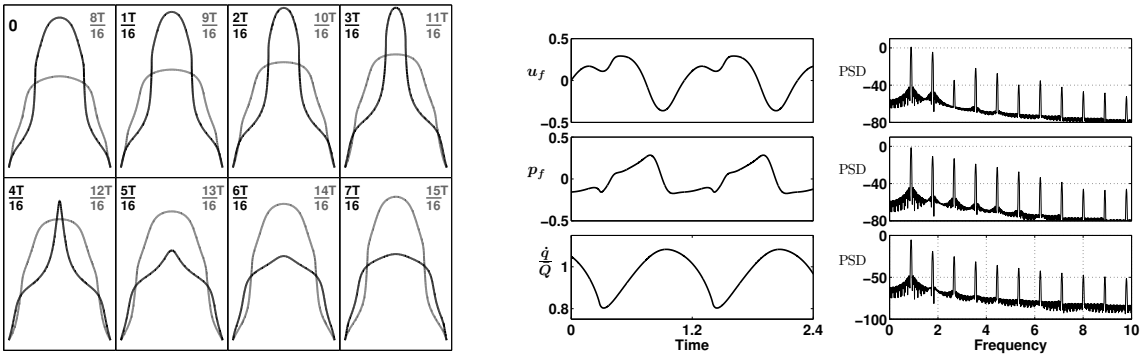

(a) (b)

Figure 6: Snapshots of the flame surface (a) and time traces and spectra (b) for the stable period-2 cycle at $x_f = 0.195$, with steady state flame aspect ratio of 4. The time scale is the same as Fig. 4.

The qualitative change in the form of the cycle along the period-2 branch can be seen using phase portraits. Figure 7 shows the phase portraits of the converged period-2 cycles at different locations along the period-2 branch of Figure 3, starting from near the Hopf bifurcation (Figure 7(a)) and moving along the branch towards towards the period-doubling bifurcation (Figure 7(t)). Because this branch of period-2 cycles is a strong function of two frequencies, it will not be captured well by frequency domain methods such as the FDF, because they consider each frequency independently.

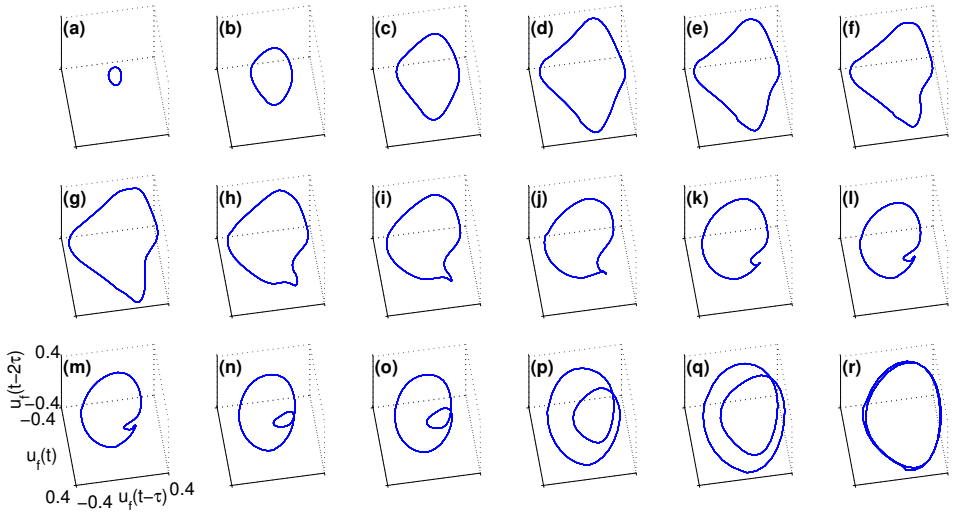

Figure 7: Phase portraits of the period-2 limit cycles at different locations along the period-2 branch of Figure 3. Near the Hopf bifurcation (a), the cycle is nearly sinusoidal with a frequency of half the fundamental acoustic mode. The cycle becomes less sinusoidal as x_f increases (b-h), because the response at the fundamental acoustic mode increases relative to the response at the half frequency. As the cycle moves closer to the period-doubling bifurcation (i-r) the phase portraits develop the familiar double loop form of a period-2 cycle, because the response of the fundamental acoustic mode is much greater than that of the half frequency. The fold bifurcation occurs between (o) and (p); the period-2 cycles (a-o) are stable, the period-2 cycles (p-r) are unstable.

2.3 Bifurcations

The Floquet multipliers describe the stability of a limit cycle to infinitesimal perturbations. Bifurcations to the limit cycle occur when a Floquet multiplier, or complex pair of Floquet multipliers, cross the unit circle. The location of the crossing point defines the type of bifurcation. The ducted premixed flame model shows several bifurcations of limit cycles: fold bifurcations, period-doubling bifurcations and Neimark-Sacker bifurcations. In all the Floquet multiplier plots of this section, the four largest magnitude Floquet multipliers are converged to 10^{-2} accuracy with the Arnoldi algorithm. The Floquet multiplier at (+1,0) is the trivial one which defines a limit cycle.

2.3.1 Fold bifurcation

A fold (LPC) bifurcation occurs when a Floquet multiplier crosses the unit circle at +1. The bifurcation changes the stability of a branch of limit cycles from stable to unstable. A fold bifurcation is observed on the period-2 branch of Figure 3 at $x_f = 0.239$. Figure 8 shows the Floquet multipliers of the period-2 cycles either side of the fold bifurcation in Figure 3, which clearly show the Floquet multiplier crossing +1. Together, the fold bifurcation at $x_f = 0.239$ and the subcritical period-doubling bifurcation at $x_f = 0.182$ create a bistable region, because between $0.182 < x_f < 0.239$ there are both stable period-1 limit cycles and stable period-2 limit cycles. Mode switching is possible in this parameter region.

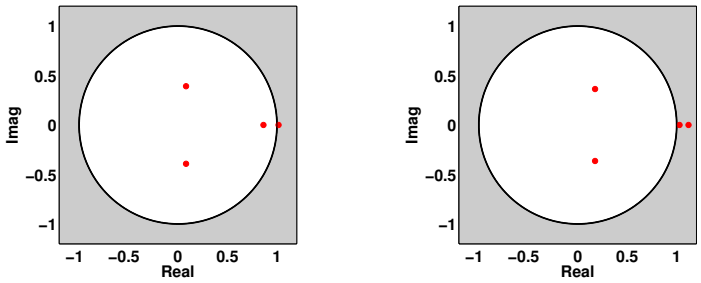

Figure 8: Floquets multipliers either side of the fold bifurcation, at $(x_f, max(u_f))$ values of $(0.239, 0.224)$ (left) and $(0.239, 0.244)$ (right). The fold bifurcation is caused by the Floquet multiplier crossing (+1,0). Only the four largest magnitude Floquet multipliers are shown.

2.3.2 Neimark-Sacker bifurcation

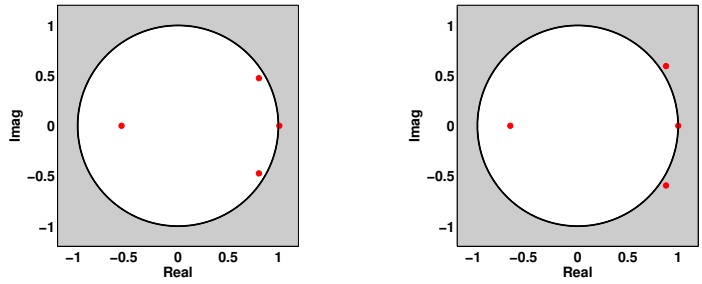

Figure 9: Floquets multipliers either side of the Neimark-Sacker bifurcation on Figure 1, at flame aspect ratio of 2.4 and x_f values of 0.2 (left) and 0.175 (right). The Neimark-Sacker bifurcation is caused by the complex conjugate pair of Floquet multipliers crossing the unit circle.

A Neimark-Sacker (torus) bifurcation occurs when a complex conjugate pair of Floquet multipliers crosses the unit circle. The bifurcation creates a branch of quasiperiodic oscillations. A quasiperiodic oscillation has two incommensurate frequencies, and therefore forms a torus in phase space. Figure

9 shows the Floquet multipliers at a limit cycle either side of the Neimark-Sacker bifurcation, which clearly show the complex pair of Floquet multipliers crossing the unit circle.

A Neimark-Sacker bifurcation can also be seen from a time series. Starting at the unstable limit cycle just after the Neimark-Sacker bifurcation, the system grows exponentially away from the limit cycle, with the peaks oscillating at a second frequency. The ratio between these two frequencies is given by the argument of the complex eigenvalue pair, divided by 2π. For the pair of Floquet multipliers in Figure 9, the ratio between the two frequencies is 10.57 (to 2d.p.). This can be seen in the time series of Figure 10, where the peaks oscillate with a period 10.57 times that of the limit cycle. It is important to note that if this number were rational, then the oscillation would be frequency locked and not quasiperiodic.

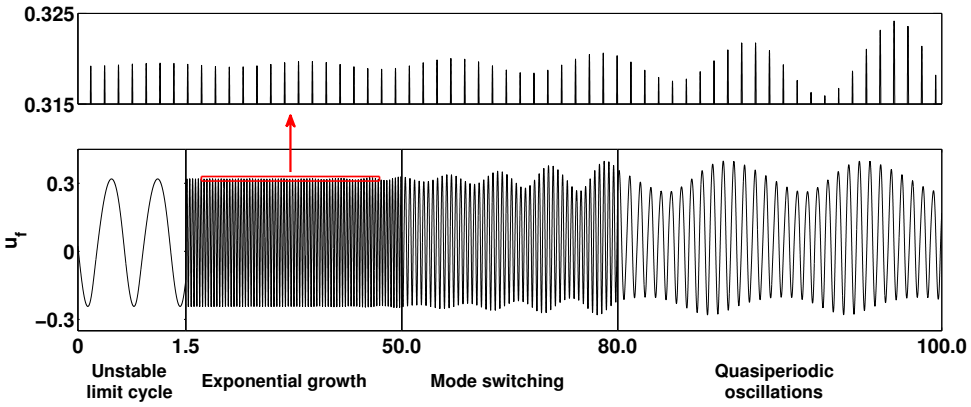

Figure 10: Time series of the system growing exponentially away from an unstable limit cycle just after a Neimark-Sacker bifurcation. The peaks oscillate at a second frequency that is defined by the argument of the pair of Floquet multipliers that cross the unit circle.

2.3.3 Period-doubling bifurcation

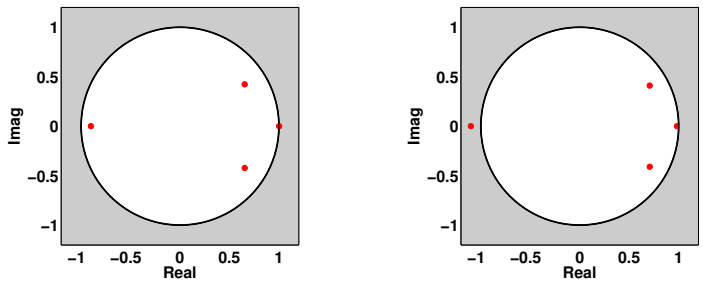

Figure 11: Floquets multipliers either side of the period-doubling bifurcation, at x_f values of 0.193 (left) and 0.175 (right). The period-doubling bifurcation is caused by the Floquet multiplier crossing (-1,0).

A period-doubling (flip) bifurcation occurs when a Floquet multiplier crosses the unit circle at -1. The bifurcation creates a branch of period-2 limit cycles, and the period-1 limit cycle becomes unstable. Figure 11 shows the Floquets multipliers at a limit cycle either side of the period-doubling bifurcation in Figure 3, which clearly show the Floquet multiplier crossing (-1,0).

A period-doubling bifurcation can also be seen from a time series (Figure 12). Starting at a the unstable limit cycle just after the period-doubling bifurcation, the system grows exponentially away from the limit cycle, with the peaks forming a characteristic one-up, one-down pattern. Because the limit cycle was converged to a high tolerance, and because the unstable Floquet multiplier is only just outside the unit circle, the system requires a long time to reach the period-2 limit cycle.

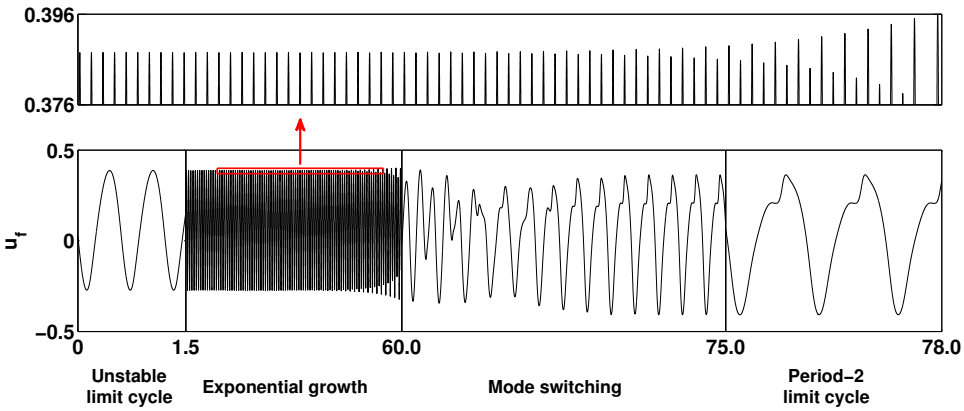

Figure 12: Time series of the system growing exponentially away from an unstable period-1 limit cycle just after a period-doubling bifurcation. The peaks form a characteristic one-up, one-down pattern. The first and the last boxes have the same scale, to show that the period-2 limit cycle has roughly twice the period of the unstable period-1 limit cycle.

The mode switching section of the time series in Figure 12 also shows that the period-doubling bifurcation is subcritical. Because the unstable limit cycle is only just beyond the period-doubling bifurcation, then if the bifurcation were supercritical, the system would quickly reach a stable period-2 limit cycle with a relatively low magnitude in the half frequency. In other words, the stable period-2 cycle would be very similar to the unstable period-1 cycle, with only a small one-up, one-down variation in the peaks and troughs.

At the period-doubling bifurcation, the Floquet mode that corresponds to the Floquet multiplier at -1 shows which coupled motion of the system is responsible for the bifurcation. This Floquet mode is shown schematically in Figure 13. At the frequency of the fundamental acoustic mode, the flame has two cusps on its surface. At half of this frequency, there should be only one cusp. The Floquet mode is a coupled motion with: (1) a flapping motion of the flame surface, where the tip and base of the flame move outwards and the middle of the flame moves inwards, coupled with (2) a variation in the velocity field every other cycle, and (3) a reduction in acoustic pressure in the duct and an increase in acoustic velocity in the duct before the flame.

3 Conclusions

Matrix-free continuation techniques were applied to a model of a ducted premixed flame. The flame model uses the kinematic G-equation, with a local level set solver. The premixed flame model has many attributes of equivalent experimental systems: the flame is axisymmetric, the flame speed is dependent on the curvature, the flame has sharp cusps, and the flame is capable of pinch-off, flashback and bulging at the burner lip. A similar ducted premixed flame model has been shown previously by Kashinath to exhibit limit cycle, period-2^n, quasiperiodic and chaotic behaviour [7], and to have many parameter regions that are multistable. These results show qualitatively the same phenomena observed in experiments by Kabiraj [1].

The continuation techniques are used to efficiently find a surface of stable and unstable limit cycles, as two system parameters vary. The continuation methods also explicitly find period-doubling and Neimark-Sacker bifurcations, by examining the Floquet multipliers of the limit cycles. A separate surface of period-2 limit cycles was found emerging from a subcritical period-doubling bifurcation. This is the first computational thermoacoustic study where period-doubling and Neimark-Sacker bifurcations have been found. The Floquet modes are examined at the bifurcations to show the coupled flame-acoustic motions that are responsible for the qualitative changes in behaviour. The continuation methods can find unstable limit cycles easily, whereas many other techniques cannot. This is important because the unstable limit cycles are crucial for mode switching [22, 7] and for separating the basins of

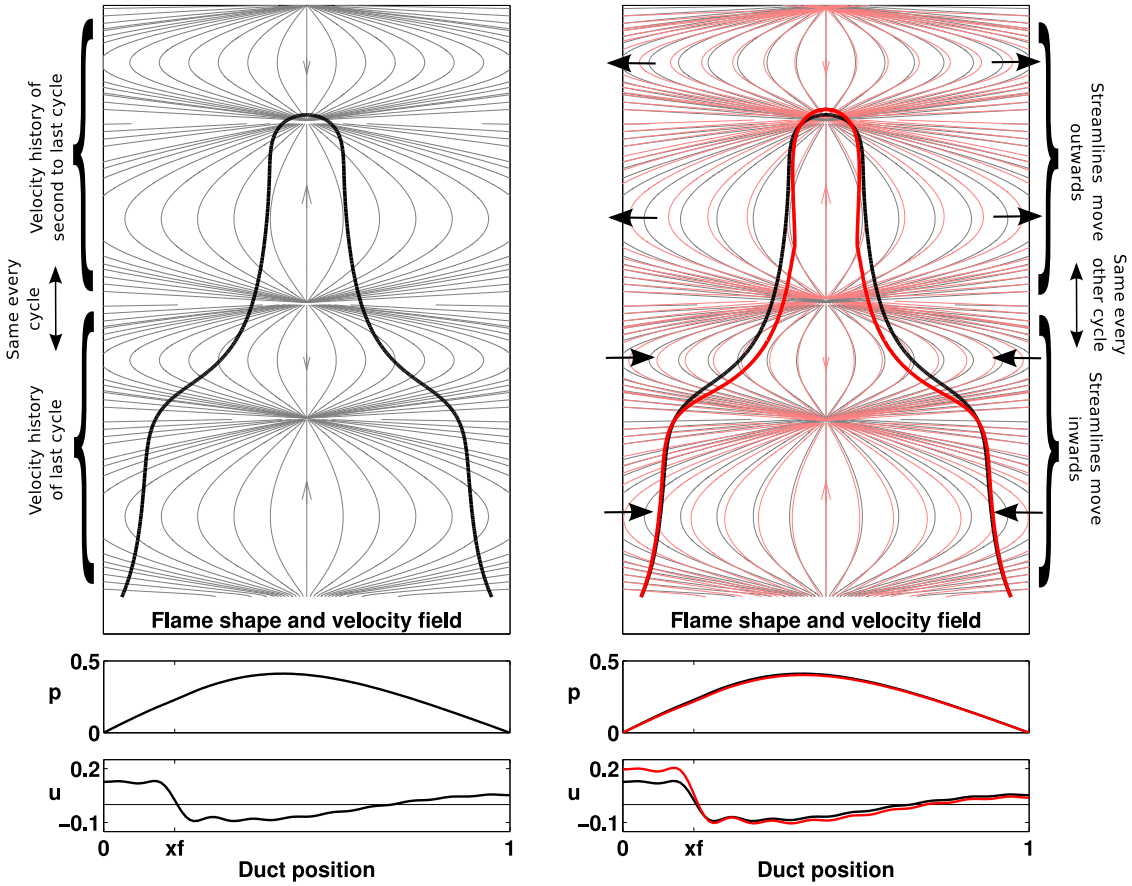

Figure 13: Floquet mode for the Floquet multiplier that causes the period-doubling bifurcation. The left hand image shows the flame shape and streamlines of the velocity field at a state on the limit cycle at the period-doubling bifurcation (aspect ratio 4). With the y-axis limits chosen, the velocity field in the lower half of the domain is repeated in the upper half of the domain - the velocity field is the history of the acoustic perturbation over the last two cycles; the last cycle corresponds to the lower half of the domain, the second to last cycle corresponds to the upper half of the domain. The right hand image shows the same as the left image (gray), superimposed with the state when perturbed a small amount in the direction of the Floquet mode that causes the period-doubling bifurcation (red). The coupled motion responsible for the period-doubling bifurcation is therefore: (1) a flapping motion of the flame surface, where the tip and base of the flame move outwards and the middle of the flame moves inwards, coupled with (2) a variation in the velocity field every other cycle, and (3) a reduction in acoustic pressure in the duct and an increase in acoustic velocity in the duct before the flame. The flame shape perturbation is scaled by a factor of two for clarity.

attraction of different attractors.

The continuation methods converge to a limit cycle by timemarching only a few cycles, but the real-time to create a bifurcation surface is governed by the speed of timemarching one cycle. Despite the LSGEN2D code being computationally expensive to timemarch, only around 14000 CPU hours were required to generate the bifurcation surfaces in this paper and to analyse the stability of the limit cycles: this is equivalent to 80 CPU cores running for one week. Because the surface is composed of several 2D slices, the process of forming a surface is easily parallelisable. For relatively little computational cost, therefore, the continuation methods can characterise the nonlinear behaviour of the coupled system over a wide parameter range.

The LSGEN2D code is able to capture the dynamics of a premixed flame under acoustic forcing, and the continuation methods are able to calculate any limit cycles and bifurcations when the flame model is coupled to an acoustic model. The results from the continuation methods could be compared with experiments in one of two ways: first, by comparing flame shapes and heat release responses; second, by comparing the self-excited behaviour and the bifurcation diagrams. With improvements to the velocity model and the acoustic model, the method described in this chapter could be an effective means of predicting and analysing the nonlinear behaviour seen in experimental premixed flame systems.

References

[1] Lipika Kabiraj, R. I. Sujith, and Pankaj Wahi. Bifurcations of Self-Excited Ducted Laminar Premixed Flames. Journal of Engineering for Gas Turbines and Power, 134(3):031502, 2012.

[2] Lipika Kabiraj, Aditya Saurabh, Pankaj Wahi, and R I Sujith. Route to chaos for combustion instability in ducted laminar premixed flames. Chaos (Woodbury, N.Y.), 22(2):023129, June 2012.

[3] Hiroshi Gotoda and Toshihisa Ueda. Transition from periodic to non-periodic motion of a bunsen-type premixed flame tip with burner rotation. Proceedings of the Combustion Institute, 29:1503–1509, 2002.

[4] Hiroshi Gotoda, Yuta Asano, Keng Hoo Chuah, and Genichiro Kushida. Nonlinear analysis on dynamic behavior of buoyancy-induced flame oscillation under swirling flow. International Journal of Heat and Mass Transfer, 52(23-24):5423–5432, November 2009.

[5] K. Kashinath, S. Hemchandra, and Matthew P. Juniper. Nonlinear Phenomena in Thermoacoustic Systems with Premixed Flames. In Proceedings of the ASME Turbo Expo, GT2012-68726, 2012.

[6] Karthik Kashinath, Santosh Hemchandra, and Matthew P Juniper. Nonlinear phenomena in thermoacoustics: A comparison betweem single-mode and multi-mode methods. In Proceedings of the 19th International Conference on Sound and Vibration, 2012.

[7] K. Kashinath, I. C. Waugh, and M. P. Juniper. Nonlinear self-excited thermoacoustic oscillations of a ducted premixed flame: bifurcations and routes to chaos. Submitted to Journal of Fluid Mechanics, 2013.

[8] A. P. Dowling. A kinematic model of a ducted flame. Journal of Fluid Mechanics, 394(September 2000):51–72, September 1999.

[9] N Noiray, D Durox, T Schuller, and S Candel. A unified framework for nonlinear combustion instability analysis based on the flame describing function. Journal of Fluid Mechanics, 615:139–167, 2008.

[10] Iain Waugh, Simon Illingworth, and Matthew Juniper. Matrix-free continuation for bifurcation analysis of large thermoacoustic systems. Journal of Computational Physics (in print), 2012.

[11] Iain Waugh. Methods for analysis of nonlinear thermoacoustic systems. PhD in Engineering, University of Cambridge, 2013.

[12] K Balasubramanian and R I Sujith. Thermoacoustic instability in a Rijke tube: Non-normality and nonlinearity. Physics of Fluids, 20:044103, 2008.

[13] Matthew P. Juniper. Triggering in the horizontal Rijke tube: non-normality, transient growth and bypass transition. Journal of Fluid Mechanics, 667:272–308, November 2010.

[14] S. Hemchandra. Dynamics of turbulent premixed flames in acoustic fields. PhD thesis, Georgia Institute of Technology, 2009.

[15] S. Hemchandra, Preetham, and Tim C. Lieuwen. Response of turbulent premixed flames to harmonic acoustic forcing. Proceedings of the Combustion Institute, 31(1):1427–1434, January 2007.

[16] Santosh Hemchandra and Tim Lieuwen. Premixed flame response to equivalence ratio perturbations. Combustion Theory and Modelling, 14(5):681–714, September 2010.

[17] Guang-Shan Jiang and Danping Peng. Weighted ENO Schemes for Hamilton–Jacobi Equations. SIAM Journal on Scientific Computing, 21(6):2126–2143, January 2000.

[18] Daniel Hartmann, Matthias Meinke, and Wolfgang Schröder. The constrained reinitialization equation for level set methods. Journal of Computational Physics, 229(5):1514–1535, March 2010.

[19] A L Birbaud, D Durox, and S Candel. Upstream flow dynamics of a laminar premixed conical flame submitted to acoustic modulations. Combustion and Flame, 146:541–552, 2006.

[20] Preetham. Modeling the response of premixed flames to flow disturbances. PhD thesis, Georgia Institute of Technology, 2007.

[21] Karthik Kashinath, Santosh Hemchandra, and Matthew Juniper. Nonlinear thermoacoustics of ducted premixed flames : the influence of perturbation convection speed. Submitted to Combustion and Flame, 2013.

[22] Iain C Waugh and Matthew P. Juniper. Triggering in a thermoacoustic system with stochastic noise. Journal of Spray and Combustion Dynamics, 3(3), 2011.